Oxidation, Reduction, and Reactivity of Supported Pd Nanoparticles: Mechanism and Microkinetics

B. Brandt, T. Schalow, M. Laurin, S. Schauermann, J. Libuda,* and H.-J. Freund

Fritz-Haber-Institut der Max-Planck-Gesellschaft, Faradayweg 4-6, 14195 Berlin, Germany

Received: September 6, 2006; In Final Form: October 11, 2006

We have studied the oxidation and reduction kinetics of Pd nanoparticles on Fe_3O_4 as well as the CO oxidation kinetics on partially oxidized Pd nanoparticles. The structural properties of the Pd/Fe_3O_4 model catalyst as well as its adsorption behavior have been studied in detail previously. Here we present the results of fully remote-controlled pulse sequence molecular beam (PSMB) experiments, using CO and O_2 molecular beams of variable intensity. It is found that at 500 K and above large quantities of oxygen are incorporated into a Pd interface oxide and, subsequently, into a Pd surface oxide. The Pd oxide coexists with metallic Pd over a broad range of conditions. We identify two reaction regimes as a function of oxygen coverage: fast CO oxidation on the O-precovered metallic Pd and slow CO oxidation involving reduction of the Pd oxide phases. The reaction orders for both reaction regimes are determined, showing a complex flux dependent behavior in the latter case. Experiments at 500 K reveal that there is a slow equilibrium between chemisorbed oxygen on the Pd metal and oxygen incorporated in the Pd oxide phases. The corresponding rate and equilibrium constants are determined, showing that at low to intermediate oxidation levels the equilibrium strongly favors the Pd oxide. As a consequence, there is a continuous depletion of chemisorbed oxygen on the metallic Pd metal at 500 K and above. An analysis of the CO oxidation kinetics on partially oxidized Pd particles in combination with microkinetic modeling suggests that the reduction of the Pd oxide is likely to proceed via two competing reaction channels: The first channel proceeds via decomposition of the oxide and release of oxygen onto the metal, followed by reaction with CO. The second channel is likely to involve a direct reaction with the oxide, possibly via a minority of active sites on the Pd oxide.

1. Introduction

Oxide-supported metal nanoparticles are commonly employed as heterogeneous catalysts for a variety of reactions.[1,2] The selectivity and activity of these systems are often found to be strongly dependent on the surface structure, particle morphology, and size, on the support, and on the presence of promoters and poisons. A particular complication arises in the case of metal nanoparticles in oxidative environments. Often the interaction of oxygen with metal surfaces and, particularly, with small metal particles turns out to be rather complex. As a result, there is an ongoing discussion on the nature of the different oxygen and oxide phases and on their activity with respect to catalytic reactions (see, for example, refs 3−6). As an example, we consider the specific case of oxygen on palladium surfaces. A large number of experimental and theoretical studies focused on this system, identifying different chemisorbed oxygen phases, subsurface oxygen species, and surface and bulk oxides.[5−24] The role of theses species in catalytic reactions is only poorly understood and some controversy remains. Hendriksen et al. studied CO oxidation on Pd surfaces using high-pressure scanning tunneling microscopy (STM), showing that oxidation of the metal surface is connected with a pronounced increase in the CO oxidation rate.[4,25] Other experimental studies on Pd single crystals show that the reaction probability of oxide phases is comparably low.[26]

The situation becomes further intricate in the cases of supported metal nanoparticles, due to the presence of different sites, such as defects, edges, corners, or different crystallographic facets, due to modified lattice constants and electronic properties and due to interaction with the support. Many of these aspects cannot be modeled on the bases of simple single-crystal studies. Therefore, we have employed nanoparticle-based model catalysts to study such effects.[5,6,22−24] For the case of Pd nanoparticles supported on ordered Fe_3O_4 films grown on Pt(111), we have recently shown that thin Pd oxide layers formed during oxygen exposure are strongly stabilized at the particle/support interface, leading to the preferential oxidation of the interface region.[22] In addition, the oxidation behavior is strongly size dependent.[24] Whereas very small particles tend to get oxidized completely, larger particles show strong kinetic hindrances with respect to interface and surface oxide formation.

Qualitatively, the following information on the oxidation behavior could be derived:[5] It could be shown that surface and interface oxides are formed from a supply of chemisorbed oxygen on metallic parts of the particle. This process of oxide formation is, in general, relatively slow in comparison to the reaction with CO. The reaction probability of CO with the oxide phases, on the other hand, was shown to be much lower than the reaction probability with chemisorbed O. Finally, it was qualitatively demonstrated that oxygen could be incorporated from the chemisorbed state into the oxide phase but also released from the oxide phase. This observation led to the conclusion that the oxide phases primarily serve as an oxygen reservoir

* Corresponding author. Present address: Lehrstuhl für Physikalische Chemie II, Universität Erlangen-Nürnberg, Egerlandstr. 3, D-91058 Erlangen, Germany. E-mail: joerg.libuda@chemie.uni-erlangen.de.

10.1021/jp0658086 CCC: $37.00
Published on Web 12/08/2006

for oxidation reactions occurring on the metallic part of the surface or at the metal oxide interface.

In the present paper we present the results of a systematic study of the elementary kinetics of Pd oxide formation on Pd nanoparticles and on the reduction kinetics of the partially oxidized Pd particles using CO. In order to study the kinetics of specific elementary reaction steps, we employ molecular beam (MB) techniques. MB methods are well-established among the methods of choice in studies of surface reaction kinetics and dynamics.[27−30] However, most studies focused on relatively simple surface reactions so far. In order to obtain detailed information on specific reaction steps of a multistep reaction system, we perform pulse-sequence molecular beam (PSMB) experiments using multiple beams. The present paper mainly focuses on this experimental approach, showing several examples and discussing the kinetic information available from the experiments. Each PSMB experiment is specifically designed to yield kinetic information on a specific step or group of steps of the reaction system. The combination of the different experiments should eventually yield a complete picture of the microkinetics of the reaction system. Finally, the results are utilized to develop a microkinetic model of the CO oxidation reaction on partially oxidized Pd nanoparticles.

2. Experimental Section

All molecular beam (MB) experiments were performed in an ultrahigh vacuum apparatus at the Fritz-Haber-Institut (Berlin), which has been described recently.[31] The system offers the experimental possibility of crossing up to three molecular beams on the sample surface.

Two effusive beams are generated by doubly differentially pumped sources based on multichannel arrays. These beams are modulated using remote-controlled shutters and valves. Opening and closing of the beams and the beam intensities are fully computer-controlled. The CO beam intensities were varied between the different experiments in a range from 8.9×10^{12} to 2.6×10^{15} molecules·cm^{-2} s^{-1} [1 Langmuir of CO (1 L; 10^{-6} Torr·s) corresponds to 3.8×10^{14} molecules·cm^{-2}]. The standard CO flux ($F_{CO,0}$) used in most experiments was 2.1×10^{14} molecules·cm^{-2} s^{-1}. Both sources were operated at room temperature. The beam diameters were chosen such that they exceed the sample diameter. All experiments have been performed using high-purity O_2 (Linde, 99.999%) and CO [Linde, 99.997% further purified by a gas filter (Mykrolis)].

The third beam is a supersonic beam, generated by a triply differentially pumped source from a supersonic expansion and modulated by a solenoid valve and a remote-controlled shutter. In this study, the supersonic source was used to generate $^{18}O_2$ beams (Campro Scientific, 95% ^{18}O, 99.7% purity) at an intensity of 4.6×10^{14} molecules·cm^{-2} s^{-1} [typical backing pressure 1.0−1.2 bar; 1 Langmuir of O_2 (1 L; 10^{-6} Torr·s) corresponds to 3.6×10^{14} molecules·cm^{-2}]. The diameter of the beam was chosen to be smaller than the sample for the experiments discussed here.

For gas-phase detection an automated quadrupole mass spectrometer (QMS) system (ABB Extrel) was employed, detecting the partial pressure of the reactants and the product C^{18}O^{16}O (46 amu). The QMS data has been checked or corrected with respect to blind experiments using catalytically inert sample surfaces. In addition, the MB apparatus allows us to acquire IR spectra (IRAS, IR reflection absorption spectroscopy) during reaction using a vacuum FT−IR spectrometer (Bruker IFS 66v/S). In this study, IR spectroscopy was used as a tool to control the reproducibility and stability of the prepared model surfaces only. For more details on IR spectroscopy on the model catalyst, see refs 5 and 32.

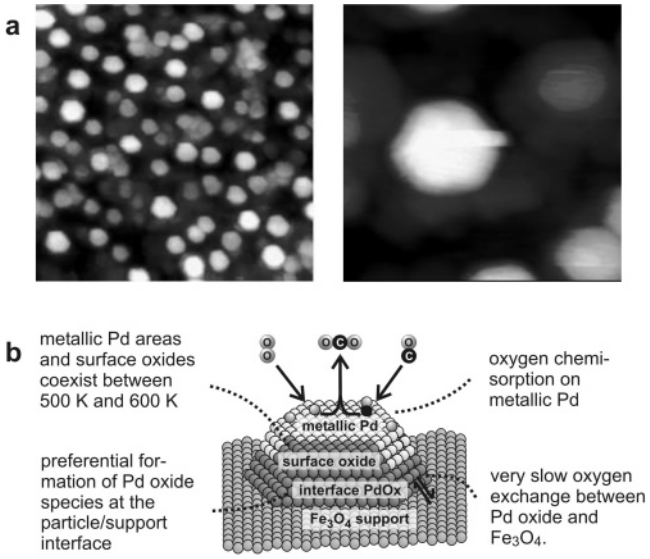

Figure 1. (a) (left) STM image of the Pd particles on Fe_3O_4/Pt(111), 100 nm × 100 nm; (right) close-up of an STM image, showing the crystalline shape of the Pd particles, 20 nm × 20 nm. Reprinted with permission from ref 22. Copyright 2005 Wiley-VCH. (b) Schematic representation of the partially oxidized Pd particles on Fe_3O_4/Pt(111).

The Pd/Fe_3O_4 model catalyst was prepared as follows: The thin (∼100 Å) Fe_3O_4 film was grown on Pt(111) by repeated cycles of Fe (>99.99%, Goodfellow) deposition and subsequent oxidation (see refs 33, 34 for details). Cleanliness and quality of the oxide film were checked by IRAS of adsorbed CO and LEED. Pd particles (>99.9%, Goodfellow) were grown by physical vapor deposition (Pd coverage 2.7×10^{15} atoms cm^{-2}, sample temperature 115 K) using a commercial evaporator (Focus, EFM 3, flux calibrated by a quartz microbalance). During Pd evaporation the sample was biased in order to avoid creation of defects by metal ions. Directly after Pd deposition, the sample was annealed to 600 K and was stabilized by a few cycles of oxygen (8×10^{-7} mbar for 1000 s) and CO exposure (8×10^{-7} mbar for 3000 s) at 500 K (compare refs 23, 33, and 34). An STM image of the model surface is shown in Figure 1a. Standard MB CO titration experiments were performed in between the MB experiments in order to control the degree of deactivation of the sample. Typically, PSMB experiments could be performed over several days before substantial deactivation of the sample was observed and preparation of a new sample was necessary.

3. Results and Discussion

3.1. Model Catalyst. As a model catalyst we have used Pd particles deposited by physical vapor deposition (PVD) on a thin, well-defined Fe_3O_4 film grown on Pt(111).[33] Growth, structure, and adsorption properties of the Pd particles and the Fe_3O_4 support have been studied in detail recently.[23,35] Most importantly, the crystalline Pd particles grow uniformly on the support (island density 8.3×10^{11} islands cm^{-2}) covering about 25% of the catalyst surface. The particles consist of ∼3000 atoms and have an average diameter of ∼7 nm. An aspect ratio of approximately 1:3.5 (height:diameter) was estimated. They expose mainly (111) facets (∼80%) but also a smaller fraction of (100) facets (∼20%) (see Figure 1a).

The qualitative oxidation and reduction behavior of the Pd particles has been characterized in a series of previous studies.[5,6,22−24] The result of this work is summarized in Figure

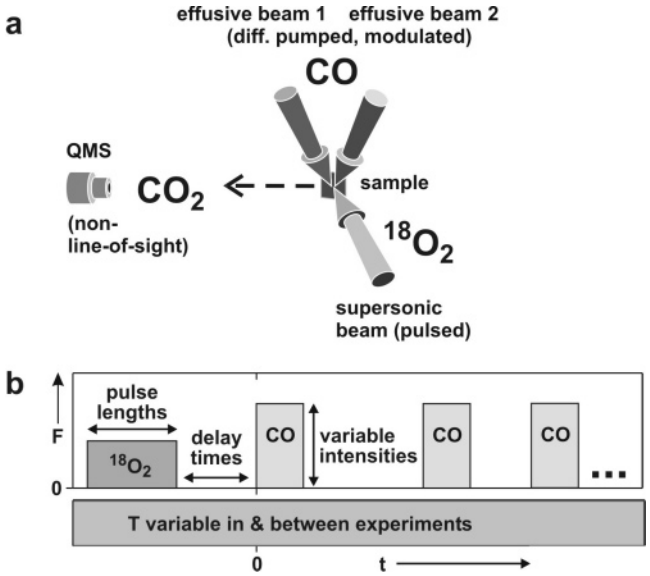

Figure 2. (a) Schematic setup of the multiple molecular beam (MB) experiment; (b) general scheme showing a typical pulse sequence molecular beam (PSMB) experiment.

1b. Under the experimental conditions applied, oxygen chemisorbs dissociatively on metallic Pd particles at temperatures below 450 K. At temperatures of 500 K and above, the particles are partially oxidized. Initial oxidation occurs at the Pd/oxide interface in the form of an interface oxide layer, stabilized by interaction with the support. Subsequently, the remaining surface of the particles can become covered by a surface oxide layer as well (the term *surface oxide* describes a very thin multilayer structure of oxygen and metal ions at the metal surface; see, for example, refs 17, 18, in the case of an *interface oxide* this structure is located at the metal/support interface). Typically, metallic and oxidized surface areas coexist over a broad range of temperatures (500−600 K). Isotope exchange experiments suggest that the rate of oxygen exchange with the Fe_3O_4 support is slow in comparison with the formation and decomposition of the Pd oxide phases. Molecular beam titration experiments furthermore indicate that the reaction probability for CO on the metallic Pd covered by chemisorbed O is much higher than the reaction probability on the Pd oxide phase. On the basis of these MB titration and sticking coefficient measurements, it was suggested that oxide formation occurs in a relatively slow process via incorporation of chemisorbed oxygen into the oxide phase. Consequently, reduction could occur via decomposition of the oxide phase and release of chemisorbed oxygen from the relatively inert oxide onto the metal. In the following, we will investigate the kinetics of the elementary steps of oxide formation and reduction employing specifically designed PSMB experiments.

3.2. The Pulse Sequence Molecular Beam Experiment (PSMB). The setup and procedure used for the PSMB experiments is schematically shown in Figure 2. Three molecular beams are superimposed on the sample surface (see Figure 2a). Two beams (effusive beams; see Experimental Section) are used to supply CO at variable flux, and the third beam is used to supply O_2 ($^{18}O_2$ is employed to reduce the level of background signals). The total formation rate of $C^{18}O^{16}O$ is recorded via a non-line-of-sight quadrupole mass spectrometer (QMS).

A typical pulse sequence is shown in Figure 2b. We start by fully reducing the Pd model catalyst by exposure to an extended pulse of CO (1800 s, not shown in the figure) at an elevated sample temperature (typically 500 K). Subsequently, the Pd

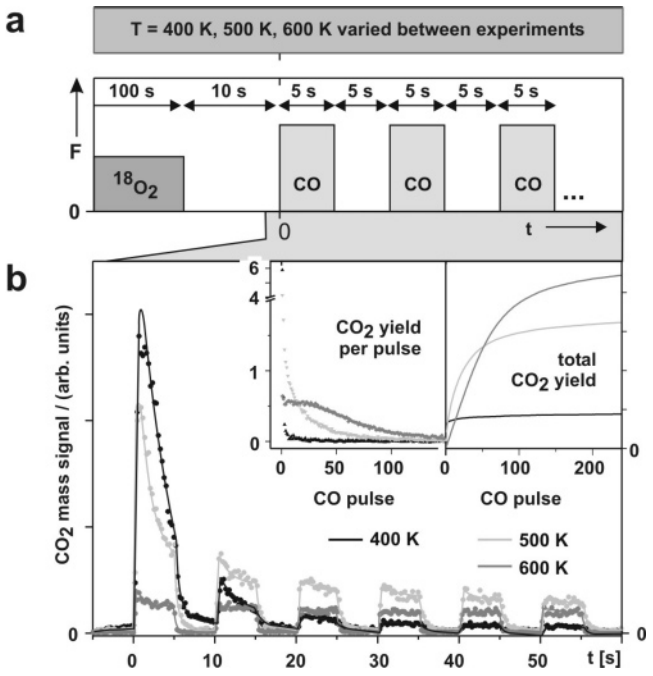

Figure 3. PSMB experiment showing the CO oxidation kinetics and quantifying the reversible oxygen uptake and release of Pd particles on Fe_3O_4/Pt(111) at different sample temperatures: (a) schematic pulse sequence ($F_{O_2} = 4.6 \times 10^{14}$ molecules·cm^{-2} s^{-1}; $F_{CO} = 2.1 \times 10^{14}$ molecules·cm^{-2}s$^{-1;}$ $T = 400$, 500, 600 K) and (b) experimental results; see text for discussion.

oxide phase is generated by exposure to a pulse of $^{18}O_2$ at the oxidation temperature T_{ox} (typically between 500 and 600 K). After changing to the reaction temperature T_r (500 K for most experiments) and after a given delay time, pulses of CO are applied. CO exposure leads to CO_2 formation, via either reaction with chemisorbed O or reduction of the oxide phases. The intensity of the CO pulses can be controlled individually as well as the delay times between the pulses. Both parameters are varied depending on the individual process to be studied. Pulse and temperature sequences as well as beam intensities are fully computer-controlled in order to ensure maximum reproducibility between the experiments.

3.3. Temperature-Dependent Oxidation and Reduction. As a first experiment, simple oxidation−reduction sequences were performed as a function of sample temperature at $T_{ox} = T_r = 400$, 500, and 600 K. Schematically, the corresponding pulse sequence is shown in Figure 3a. After full reduction of the Pd model catalyst by an extended CO pulse (duration = 1800 s, $T_r = 500$ K), an oxygen pulse (4.6×10^{14} molecules·cm^{-2} s^{-1}, $t = 100$ s) is applied in order to form some amount of Pd oxide. Following a delay time (10 s), 240 CO pulses (pulse duration = 5 s, 2.1×10^{14} molecules·cm^{-2} s^{-1}, delay between pulses = 5 s) are applied.

In Figure 3b the CO_2 formation rate that is obtained as a response to the CO pulses is displayed. The two insets show the CO_2 yield per pulse and the total CO_2 yield up to a given pulse.

We consider the behavior at $T_{ox} = T_r = 400$ K first. At this temperature it is known that there is practically no formation of Pd oxides but chemisorption of O on metallic Pd only.[5] It is observed that the CO_2 formation rate during the first CO pulse is very high, but within a few pulses it decreases rapidly below the detection limit. In accordance with previous MB experiments on the CO oxidation on Pd particles, this result shows that the reaction probability for CO on O-precovered Pd particles is high

(compare, refs 36 and 37). The total CO_2 yield can thus be directly associated with the chemisorption capacity of the Pd particles. Assuming saturation coverages of $\theta = 0.25$ and $\theta = 0.5$ for Pd(111)[7] and Pd(100),[38] respectively, and assuming 80% (111) facets and 20% (100) facets, we obtain an estimate of $\theta = 0.3$ for the average oxygen coverage on the particle surface.

We now turn to the behavior upon oxygen exposure at higher temperature. Note that with increasing oxidation temperature the degree of oxidation of the Pd particles rapidly increases at 500 K and above.[5] In the pulsed reduction experiment two effects are observed. First, the initial CO_2 formation rate during the first CO pulse decreases with increasing oxidation temperature; second, the CO_2 formation rate remains finite over a large number of pulses, leading to a nearly 5-fold increase of the total CO_2 yield at 600 K in comparison to the experiment at 400 K. This large oxygen release in not compatible with surface adsorption but can be associated with the reversible formation of interface and surface oxides on the Pd particles (see ref 5 for a more detailed discussion). By comparison with the titration experiment at 400 K, we can assign the intense CO_2 formation peak during the first CO pulse to the reaction of CO with chemisorbed oxygen on the Pd metal, whereas the CO production in the subsequent pulses is associated with the reduction of the Pd oxide itself.

With respect to the Pd oxide reduction kinetics, two points are of particular importance: First, it is apparent from the low CO_2 formation rate in the Pd oxide reduction regime that the reduction of the Pd oxide by CO is a slow process in comparison with the reaction of CO with chemisorbed oxygen. Second, from the decreasing amplitude of the first CO_2 peak with increasing oxidation temperature, it can be concluded that the reaction probability for CO on the oxidized surface is by far lower as compared to the reaction probability of CO impinging on the oxygen-precovered metallic surface.

With respect to a quantitative comparison of the reaction probabilities, a weak point of the specific experiment in Figure 3 is the fact that the reduction is performed at different temperatures. In order to probe the reaction probabilities as a function of the degree of oxidation, but at constant reaction temperature, a second type of experiment is performed (see Figure 4a): Again the oxidation is carried out by applying an oxygen pulse (t = 100s, 4.6×10^{14} molecules·cm^{-2} s^{-1}) at different oxidation temperatures (T_{ox} = 500, 600 K). From previous work it is known that at 500 K interface oxide is preferentially formed, whereas upon oxidation at 600 K a large fraction of the particle surface becomes covered by a surface oxide.[5] Subsequent to oxidation the sample is cooled in the oxygen beam to a reaction temperature of T_{red} = 500 K and a pulse titration experiment is performed (pulse duration = 5 s, 1.0×10^{15} molecules·cm^{-2} s^{-1}, delay between pulses = 5 s). The experimental result is displayed in Figure 4b. Similar to the experiment shown in Figure 3, the CO_2 production can be subdivided into an initial peak originating from chemisorbed O on metallic Pd and from a slowly decreasing component that can be assigned to the reduction of the Pd oxide. The total amount of CO_2 originating from Pd oxide is larger for oxidation at 600 K (see the inset in Figure 3b). The initial reaction probability for the sample that has been oxidized at 600 K is substantially lower than for oxidation at 500 K, however. This result shows clearly that, under otherwise identical conditions, the reaction probability for CO impinging on oxidized Pd is considerably lower than for chemisorbed O on metallic Pd. Another important point concerns the reaction rate in the oxide reduction region, which is initially lower at a higher degree of surface oxidation. This observation points to a relatively complex reduction mechanism, only involving part of the oxide surface sites. In section 3.6, we will discuss the possible mechanisms in detail.

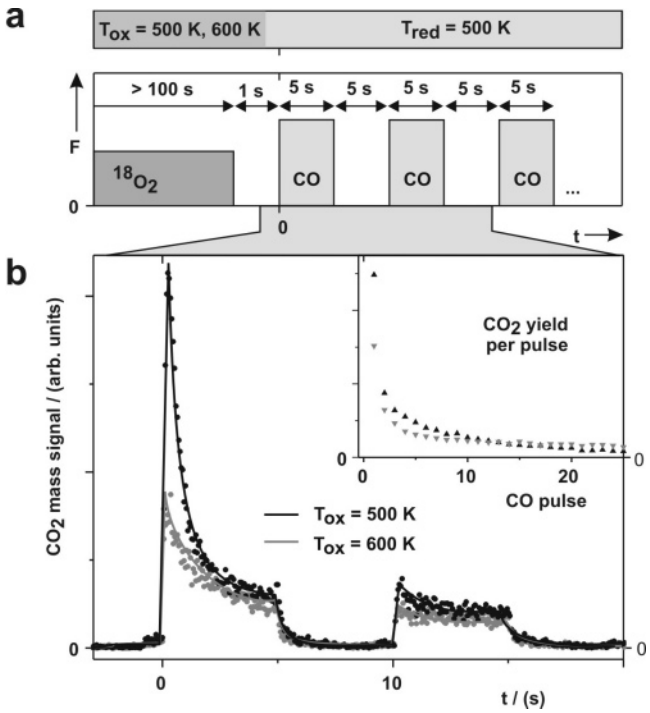

Figure 4. PSMB experiment showing the CO oxidation kinetics at 500 K on Pd particles on Fe_3O_4/Pt(111) after partial oxidation at different sample temperatures (500 K, 600 K): (a) schematic pulse sequence ($F_{O_2} = 4.6 \times 10^{14}$ molecules·cm^{-2}·s^{-1}; $F_{CO} = 1.0 \times 10^{15}$ molecules·cm^{-2}·s^{-1}) and (b) experimental results, see text for discussion.

3.4. Determination of Reaction Orders of Reaction Channels. In the previous section, it has been shown that during a CO pulse titration experiment the CO_2 production can be subdivided into two regimes, i.e., into the reaction of chemisorbed O on metallic Pd with CO and the regime in which the Pd oxide phase is reduced. As a next step, we try to obtain additional information on the kinetics of the two reaction regimes by determining the reaction order with respect to CO.

To start with, we focus on the first reaction channel, i.e., the reaction with chemisorbed oxygen. Similar as described before, the experimental procedure (see Figure 5a) involves the complete reduction of the sample by an extended CO pulse (500 K), followed by an oxidation pulse at 500 K (4.6×10^{14} molecules·cm^{-2} s^{-1}, t = 100 s). After a delay time (1 s), the adsorbed oxygen is titrated by CO pulses (pulse duration = 5 s, $F_{CO,0} = 2.1 \times 10^{14}$ molecules·cm^{-2} s^{-1}, delay between pulses = 5 s). In contrast to the previously described experiments, however, the CO flux is varied over more than 2 orders of magnitude. The result of the experiment is shown in Figure 5b. It is found that the initial rate of CO_2 production is strongly dependent on the CO flux. A more quantitative analysis is shown in the inset, in which the initial CO_2 formation rate is plotted as a function of the CO flux (log−log plot). A fit yields a reaction order of 0.9 ± 0.1 in CO. This result is in agreement with the interpretation that the initial CO_2 peak is due to reaction of CO with preadsorbed oxygen on Pd metal. In the limit of high oxygen precoverage, we expect a high reaction probability for CO to CO_2. Under these conditions CO adsorption is the rate-limiting step of the reaction, and the rate is proportional to the CO flux (see ref 39 and also discussion in ref 30).

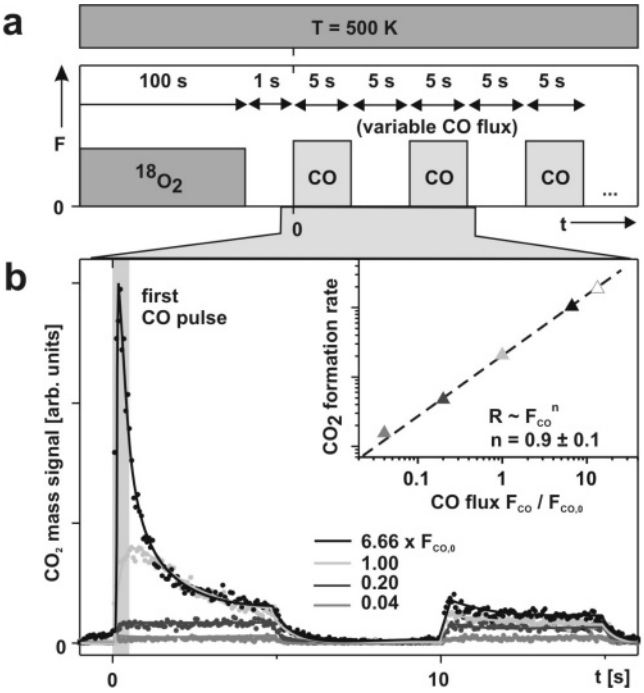

Figure 5. PSMB experiment for determination of the CO reaction order for CO oxidation involving chemisorbed oxygen on metallic Pd. The experiment is performed at 500 K on Pd particles on Fe_3O_4/Pt(111) after partial oxidation at 500 K; (a) schematic pulse sequence (F_{O_2} = 4.6×10^{14} molecules·cm^{-2}·s^{-1}; $F_{CO,0} = 2.1 \times 10^{14}$ molecules·cm^{-2}·s^{-1}) and (b) experimental results; see the text for discussion.

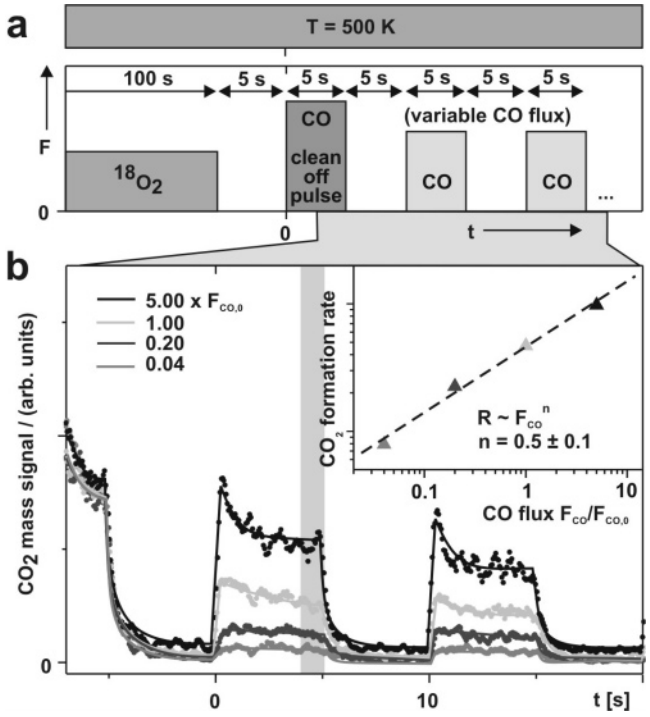

Figure 6. PSMB experiment for determination of the CO reaction order for CO oxidation involving Pd oxide phases. The experiment is performed at 500 K on Pd particles on Fe_3O_4/Pt(111) after partial oxidation at 500 K; (a) schematic pulse sequence ($F_{O_2} = 4.6 \times 10^{14}$ molecules·cm^{-2}·s^{-1}; $F_{CO,0} = 2.1 \times 10^{14}$ molecules·cm^{-2}·s^{-1}) and (b) experimental results; see the text for discussion.

If we now turn our attention to the CO_2 production during the subsequent CO pulses, i.e., to the regime that is assigned to the Pd oxide reduction, we find substantially weaker flux dependence as for the initial CO pulse. In order to analyze the reaction order in this regime more quantitatively, a second type of flux-dependent experiment is performed (see Figure 6a): As before, we start by fully reducing the sample and preparing a well-defined amount of Pd oxide by exposure to an O_2 pulse of defined length. Subsequently, one very intense CO pulse is applied, which removes the chemisorbed oxygen completely. This step ensures that the conditions at this point of the experiment are always identical. Subsequently, a series of CO pulses with different intensities are used in order to probe the flux dependence in the oxide reduction regime. The result is shown in Figure 6b. We find a reaction order for CO that varies between approximately 0.4 and 0.6 in the flux regime probed in this experiment. The fractional order of the reaction rate with respect to the CO flux indicates a complex reaction mechanism. We may assume that the decomposition of the Pd oxide may contribute to the rate control of the reaction. In section 3.6, we will develop a detailed kinetic model that is capable of reproducing the flux dependence shown in Figures 5 and 6.

3.5. Formation and Decomposition Kinetics of the Pd Oxide Phase. Before discussion of the possible models for CO oxidation on partially oxidized Pd particles, however, we will first consider some experiments thay are capable of providing detailed experimental information on the oxidation and reduction kinetics.

The first experiment, which addresses the formation of Pd oxides from chemisorbed oxygen, is shown in Figure 7. Here, the fully reduced sample is exposed to a short pulse of oxygen (4.6×10^{14} molecules·cm^{-2} s^{-1}, $t = 2$ s). This pulse leads to a high coverage of chemisorbed oxygen on metallic Pd, but it is too short to lead to substantial oxidation of the Pd particles. After a variable delay time (1−100 s) the remaining oxygen

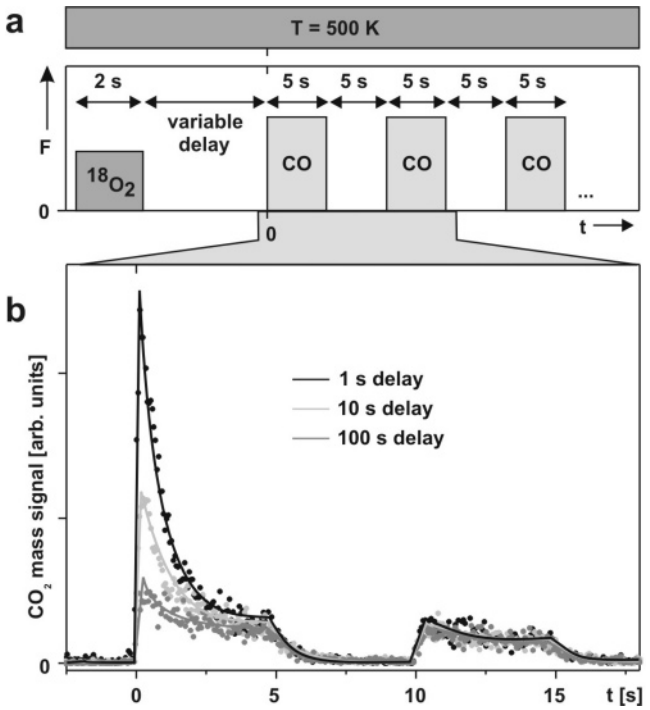

Figure 7. PSMB experiment showing the depletion of chemisorbed oxygen on metallic Pd as a function of time due to Pd oxide formation. The experiment is performed at 500 K on Pd particles on Fe_3O_4/Pt-(111); (a) schematic pulse sequence ($F_{O_2} = 4.6 \times 10^{14}$ molecules·cm^{-2}·s^{-1}; $F_{CO,0} = 2.1 \times 10^{14}$ molecules·cm^{-2}·s^{-1}) and (b) experimental results; see the text for discussion.

on the sample is titrated by pulses of CO (pulse duration = 5 s, 2.1×10^{14} molecules·cm^{-2} s^{-1}, delay between pulses = 5 s). We observe that with increasing delay time the intensity of the CO_2 peak during the first CO pulse decreases rapidly

In line with the discussion in the previous section, we conclude from this observation that during the delay period chemisorbed oxygen is removed from the Pd metal by incorporation into the Pd oxide phase (on the basis of blind experiments and considering the present temperature range we can exclude background reaction and desorption as possible reasons for oxygen depletion). There are two implications connected to this observation, which are noteworthy. First, it follows that the formation of the Pd oxide phase is a relatively slow process. This is in agreement with previous pulsed sticking coefficient measurements.[5] Second, it can be concluded that the formation of Pd oxide phases appears to be much more facile than on single-crystal surfaces. On the latter, theoretical calculations by Reuter, Scheffler, and co-workers[18−20] and as well as experimental investigations[17−19] suggest that surface oxides are only formed at high oxygen coverage. In contrast to this, the pulse delay experiment on Pd particles shown in Figure 7 suggests that the chemisorbed oxygen is nearly completely incorporated into the oxide phase after a delay time of 100 s. This observation supports the hypothesis that the oxide phases formed of the Pd nanoparticles may be strongly stabilized due to the limited particle size and, more importantly, by interaction with the support. In addition, kinetic hindrances for oxidation may be partially lifted on supported particle systems, as also shown in recent work by Kasper et al.[40]

A close inspection of the shape of the second CO_2 pulse in Figure 6 reveals another interesting piece of information: Especially for high CO flux, the CO_2 production in the second pulse and in following pulses shows a typical overshooting behavior, i.e., immediately after admission of the CO beam pulse a high rate of CO_2 production is observed, which exceeds the pseudo-steady-state reaction rate level reached in the previous pulse.

In view of the delay experiment in Figure 7, we may anticipate that this overshooting could be associated with some chemisorbed oxygen on Pd metal or some other reactive oxygen minority species that migrates back from the oxide phase in the absence of CO. This observation suggests that there is a dynamic equilibrium of oxygen chemisorbed on the metal and oxygen incorporated into the oxide phase. If this is indeed the case, it should, however, not only be possible to monitor the depletion of chemisorbed oxygen upon incorporation into the oxide phase but also the release of oxygen onto the metallic part of the surface upon decomposition of the oxide phase.

The corresponding pulse sequence experiment resolving the decomposition kinetics is illustrated in Figure 8a: Again, the fully reduced sample is exposed to a short pulse of oxygen (4.6×10^{14} molecules·cm^{-2} s^{-1}, $t = 100$ s). During this pulse a well-defined amount of Pd oxide is formed, while the remaining fraction of metallic Pd remains completely covered by chemisorbed oxygen. After a delay time (10 s) we now apply one intense CO pulse (pulse duration = 10 s, 1.1×10^{15} molecules·cm^{-2} s^{-1}) in order to remove the chemisorbed oxygen completely (oxygen-clean-off pulse, no significant Pd oxide reduction occurs on this short time scale). After a variable delay time ($t = 0.5-150$ s) a series of further CO pulses is applied (pulse duration = 10 s, 1.1×10^{15} molecules·cm^{-2} s^{-1}) and the CO_2 production is recorded. It is found that the pulse shape in the first pulse after the variable delay shows a characteristic dependence on the delay time. For very short delays, there is no overshooting of the CO_2 signal, whereas the characteristic CO_2 overshooting peak appears at longer delay times, typically on a characteristic time scale of about 5 s.

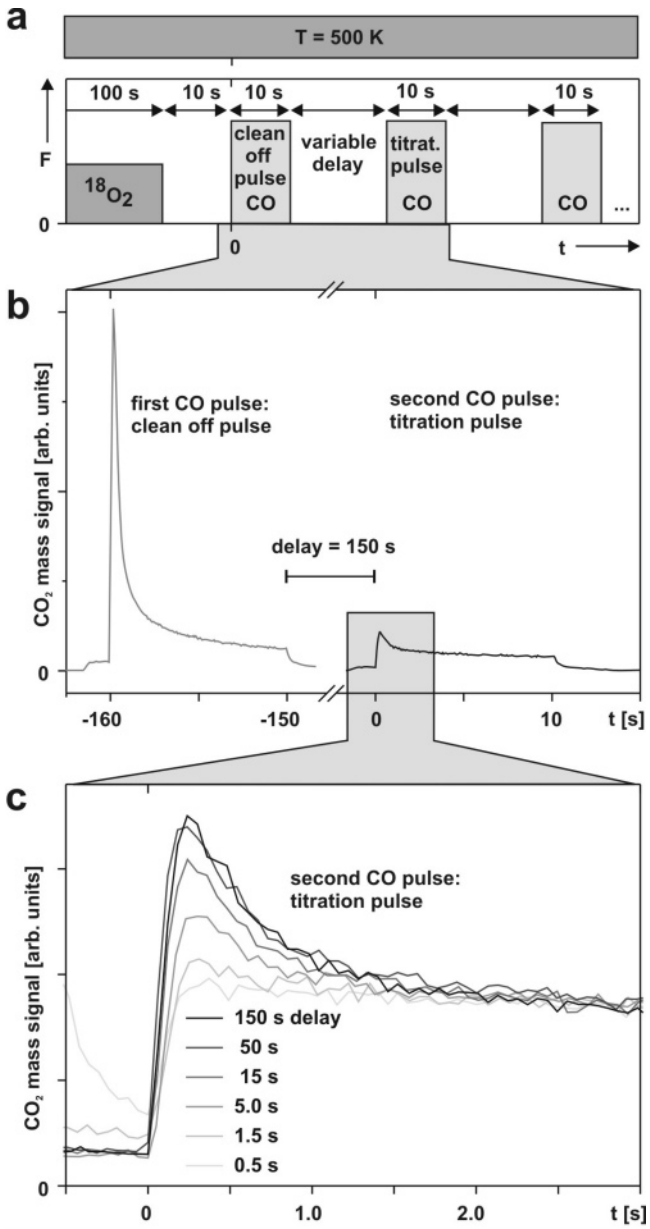

Figure 8. PSMB experiment showing the decomposition kinetics of the Pd oxide phases and the release of oxygen upon reduction with CO. The experiment is performed at 500 K on Pd particles on Fe_3O_4/Pt(111) after partial oxidation at 500 K; (a) schematic pulse sequence ($F_{O_2} = 4.6 \times 10^{14}$ molecules·cm^{-2}s^{-1}; $F_{CO} = 1.0 \times 10^{15}$ molecules·cm^{-2}·s^{-1}) and (b) experimental results; see the text for discussion.

We assign this behavior to the decomposition of the Pd oxide phase and the release of oxygen from the oxide onto the Pd metal. It should be noted that after approximately 50 s the equilibrium coverage of oxygen on the metallic Pd is nearly reached. A rough estimate of the oxygen coverage on the Pd metal in equilibrium with the Pd oxide phase can be obtained by a comparison of the peak height in the second pulse in comparison with the first (oxygen-clean-off) pulse. We obtain an equilibrium oxygen coverage corresponding to about 6.5% of the O saturation coverage on metallic Pd.

3.6. Microkinetic Modeling. Finally, we analyze the results of the PSMB experiments described in the previous sections in terms of simple microkinetic models. The idea at this stage is to qualitatively identify the role of oxide formation on Pd particles for the kinetics of CO oxidation. Moreover, we would like to identify the elementary steps that are essential with

respect to a microkinetic description of the CO oxidation on partially oxidized noble metal particles. Naturally, a more complete model would also have to incorporate dependencies on oxide coverage and reaction temperature. Such extended models require an even broader set of experimental data but may become available in future studies.

Our present kinetic model is based on the microkinetic description of Hoffmann et al.[37,41] used for the simulation of transient and steady-state MB experiments on the CO oxidation on Pd nanoparticles. In addition to the elementary steps of this model, i.e., CO adsorption and desorption, dissociative O_2 adsorption, and the Langmuir−Hinshelwood (LH) surface reaction between CO and O, we include the formation and decomposition of oxide phases. In a hierarchical fashion, models of increasing complexity are constructed and tested with respect to their compatibility with the experimental results. Schematically, these models are summarized in Figure 9. In the following we will describe and discuss these models and their implications in detail.

Model 1: Reversible Formation of an Inert Oxide Phase. In the first model, we assume that CO oxidation occurs on the metallic Pd phase only. In order to describe the microkinetics of CO oxidation, we use the model and parameters of Hoffmann et al.[41] The Pd oxide phase is assumed to serve as a pure oxygen reservoir only. With these assumptions we obtain for the CO and O coverage:

$$\frac{\mathrm{d}\theta_{\mathrm{O(ad)}}}{\mathrm{d}t} = 2\cdot\frac{F_{\mathrm{O_2}}}{N_{\mathrm{Pd}}}\cdot S_{\mathrm{O_2}} - f_{\mathrm{f,Ox}}\theta_{\mathrm{O(ad)}} + f_{\mathrm{d,Ox}}\theta_{*} - k_{\mathrm{LH}}\theta_{\mathrm{O(ad)}}\theta_{\mathrm{CO}} \tag{1}$$

$$\frac{\mathrm{d}\theta_{\mathrm{CO}}}{\mathrm{d}t} = \frac{F_{\mathrm{CO}}}{N_{\mathrm{Pd}}}\cdot S_{\mathrm{CO}} - k_{\mathrm{des,CO}}\theta_{\mathrm{CO}} - k_{\mathrm{LH}}\theta_{\mathrm{O(ad)}}\theta_{\mathrm{CO}} \tag{2}$$

The reaction rate (per Pd surface site) is described by

$$r_{\mathrm{CO_2}} = k_{\mathrm{LH}}\theta_{\mathrm{O(ad)}}\theta_{\mathrm{CO}} \tag{3}$$

Here $\theta_{\mathrm{O(ad)}}$ and θ_{CO} are the coverages of chemisorbed O and CO, respectively, $F_{\mathrm{O_2}}$ and F_{CO} are the beam fluxes, $S_{\mathrm{O_2}}$ and S_{CO} are the sticking coefficients, $k_{\mathrm{des,CO}}$ and k_{LH} are the rate constants for the CO desorption and the LH surface reaction, and N_{Pd} is the density of Pd surface atoms (1.53×10^{15} cm^{-2}). For all parameters and their temperature and coverage dependencies (see ref 41). The second and third terms in eq 1 describe the formation and decomposition of the oxide phase. The Pd oxide is assumed to be formed by incorporation of chemisorbed oxygen into the oxide phase, and decomposition is assumed to result in release of oxygen onto the metallic surface. Therefore, we anticipate in our model that the rate of oxide formation is proportional to the coverage of chemisorbed oxygen on the Pd metal ($\theta_{\mathrm{O(ad)}}$), and the rate of decomposition is proportional to the coverage of empty sites (θ_*) with

$$\theta^* = \left(1 - \frac{\theta_{\mathrm{O(ad)}}}{\theta_{\mathrm{O(ad),max}}} - \frac{\theta_{\mathrm{CO}}}{\theta_{\mathrm{CO,max}}}\right) \tag{4}$$

The functions $f_{\mathrm{f,Ox}}$ and $f_{\mathrm{d,Ox}}$ contain all other dependencies of the oxide formation and decomposition rates. These rates should be proportional to the number of boundary sites between the two phases, if the oxide formation occurs via the metal oxide boundary. However, we know that primarily interface oxide is formed over the range of conditions investigated here, which motivates the assumption that the rate should be constant to a first approximation. This assumption is well-justified at least over a limited range of oxide coverages, whereas over a broad range of oxide coverages, a more elaborate model may have to be developed. Finally, we take into account that oxide formation

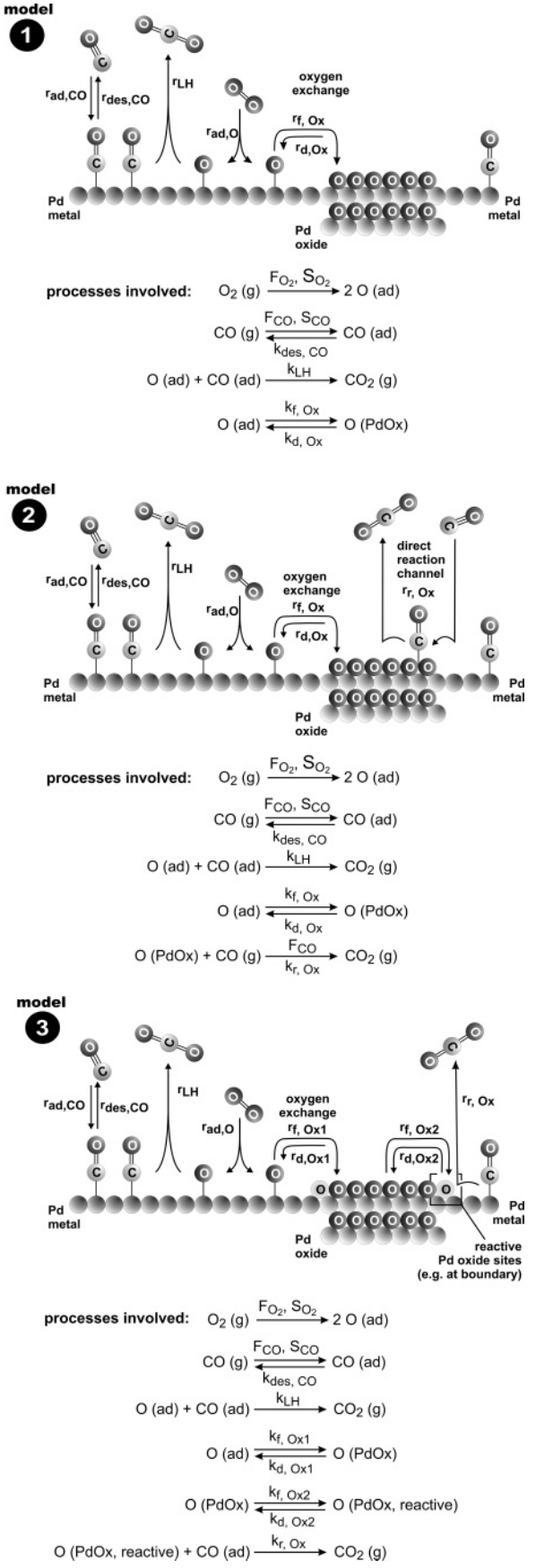

Figure 9. Microkinetic models for CO oxidation on partially oxidized Pd particles (see the text).

nearly stops at a certain maximum oxide coverage $\theta_{O(PdOx)}$ (see, for example, ref 5; the amount of oxide formed depends on the oxidation temperature). Therefore, we describe the rates of oxide formation and decomposition as

(oxide formation)

$$f_{f,Ox}\theta_{O(ad)} = \begin{cases} k_{f,Ox}\theta_{O(ad)} & ;\theta_{O(PdOx)} < \theta_{O(PdOx),max} \\ 0 & ;\theta_{O(PdOx)} \geq \theta_{O(PdOx),max} \end{cases} \quad (5)$$

(oxide decomposition)

$$f_{d,Ox}\theta_{*} = \begin{cases} k_{d,Ox}\theta_{*} & ;\theta_{O(PdOx)} \geq 0 \\ 0 & ;\theta_{O(PdOx)} < 0 \end{cases} \quad (6)$$

This yields, for the change in Pd oxide coverage as a function of time,

$$\frac{d\theta_{O(PdOx)}}{dt} = f_{f,Ox}\theta_{O(ad)} - f_{d,Ox}\theta_{*} \quad (7)$$

The only unknown parameters in this model are the rate constants that describe the formation and decomposition of Pd oxide, $k_{f,Ox}$ and $k_{d,Ox}$. These two parameters can be directly extracted from the PSMB experiment displayed in Figure 8: after complete removal of chemisorbed O in the first CO pulse, chemisorbed oxygen is formed again by decomposition of the Pd oxide. The initial rate of this oxygen release is determined by $k_{d,Ox}$ only. This constant can therefore be directly extracted from the rate of oxygen release at low delay times (compare Figure 8c). The second rate constant can be determined, if we take into account that the ratio of the two rate constants $k_{f,Ox}$ and $k_{d,Ox}$ determines the coverage of chemisorbed oxygen in equilibrium with the Pd oxide phase. If we consider the CO_2 response to the first two CO pulses as displayed in Figure 8b, we may assume that the response to the first pulse to a first approximation corresponds to the saturation coverage of chemisorbed oxygen. From the size of the CO_2 peak in the second pulse after long delay times, it can be concluded that the coverage of chemisorbed O in equilibrium with the oxide phase corresponds to a few percent of saturation coverage only. These considerations show that the two rate constants are independently determined by the experiment. The exact values can be extracted by simulating the complete PSMB experiment. Such a simulation yields $k_{f,Ox} = 0.09\ s^{-1}$ and $k_{d,Ox} = 0.000\ 72\ s^{-1}$.

Now that all kinetic parameters are determined, we may test the model for consistency with other experiments by simulating the full PSMB data in Figures 8 and 6. The results of these simulations are shown in the topmost panels of Figures 10 and 11.

A direct comparison between the PSMB experiment in Figure 8 and the simulation using model 1 is shown in Figure 10. It is found that the delay time dependence of the CO_2 peak is reproduced well. Also the ratio between the first and the second CO_2 pulse is described well by the model. A close inspection shows, however, that there is at least one feature of the experiment that is entirely incorrectly predicted by the model: whereas the simulation predicts a decrease of the CO_2 production rate after the initial peak to a very low value, the experimental data show that the CO_2 production remains at a high pseudo-steady-state level continuously. This high reaction rate cannot be accounted for by the simple storage and release model of type 1. A second indication that the model is not describing the behavior properly is derived from comparison with the PSMB experiment in Figure 6. Here the flux dependence of the oxide reduction channel is probed. The comparison in Figure 11 shows that the simple storage and release model predicts a pronounced saturation behavior as a function of the CO flux, which is not observed experimentally. From this we conclude

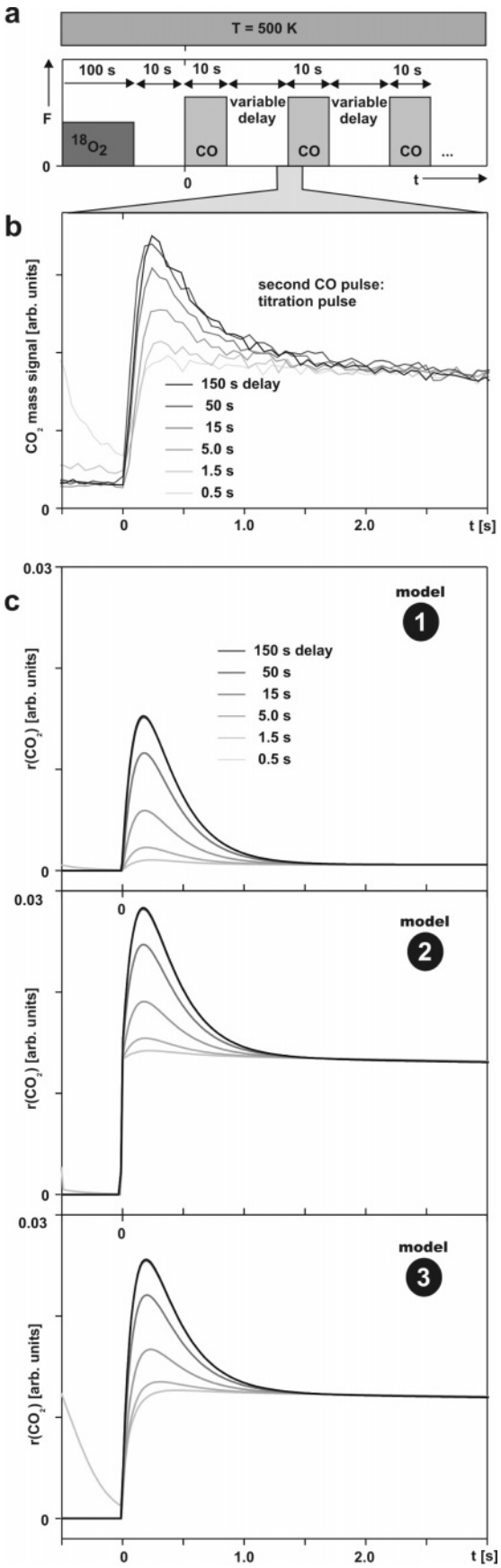

Figure 10. Comparison of the PSMB experiment on the decomposition kinetics of the Pd oxide phases (Figure 8) to the predictions based on microkinetic models 1−3 (see the text).

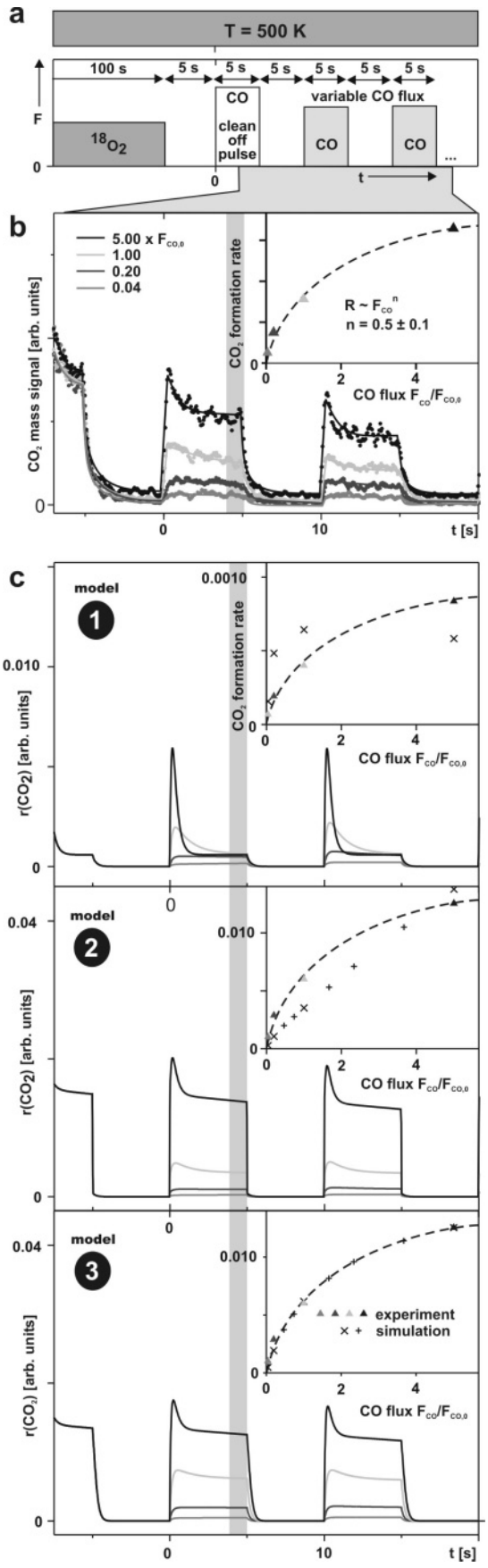

Figure 11. Comparison of the PSMB experiment for determination of the CO reaction order for CO oxidation involving Pd oxide phases (Figure 6) to the predictions based on microkinetic models 1−3 (see the text).

that the simple model 1, treating the Pd oxide as an inert oxygen reservoir, is not sufficient. Instead a second reaction channel involving a direct reaction of CO with the oxide has to be taken into account.

Model 2: Reversible Formation of an Oxide Phase with Low Activity. Due to the incompatibility of model 1 with the experimental data, we extend this model by considering a direct reaction of CO with the oxide as an additional reaction channel. With these assumption, eqs 3 and 7 are transformed into

$$\frac{d\theta_{O(PdOx)}}{dt} = f_{f,Ox}\theta_{O(ad)} - f_{d,Ox}\theta_* - \frac{F_{CO}}{N_{Pd}}k_{r,Ox}\theta_{O(PdOx)} \quad (8)$$

$$r_{CO2} = k_{LH}\theta_{O(ad)}\theta_{CO} + \frac{F_{CO}}{N_{Pd}}k_{r,Ox}\theta_{O(PdOx)} \quad (9)$$

The last term in these equations describes the direct reaction of the oxide with adsorbed CO. Here we assume (in accordance with the experimental data[5]) that adsorption of CO on the Pd oxide is weak, leading to a linear dependence of the CO coverage on the oxide on the CO flux. Under these conditions, a first-order dependence of the rate on the CO flux is expected. $k_{r,Ox}$ is the effective rate constant for the direct reaction channel of adsorbed CO with the Pd oxide phase, i.e., without decomposition of the oxide and release of oxygen onto the metal. The value of this rate constant can be directly determined from the PSMB experiment shown in Figure 8. Apparently, the direct reaction must be solely responsible for the enhanced pseudo-steady-state reaction rate after decay of the initial CO_2 peak. Keeping all constants from model 1 fixed, we derive $k_{r,Ox}$ from simulations, which are fitted to the experimental data. In this manner, we obtain a value of $k_{r,Ox} = 0.023$. The result of the simulation is shown in Figure 10. We find that the PSMB experiment in Figure 8 is now well reproduced by model 2.

A shortcoming of model 2 becomes apparent, however, if we try to simulate the flux dependence of the oxide reduction rate (PSMB experiment in Figure 6) by model 2: The model predicts a direct reaction channel that is first order in the CO partial pressure. As a consequence, the reaction rate is expected to be dominated by this channel at high CO pressure. In contrast to this prediction, the experiment shows a characteristic saturation behavior instead. We summarize at this point that the reduction kinetics points to the presence of two reaction channels, i.e., (i) a decomposition channel releasing oxygen onto the Pd metal where it reacts with chemisorbed CO and (ii) a direct reaction channel of CO involving the oxide. The kinetics of the latter appears to be relatively complex, however, possibly indicating the presence of different oxide sites.

Model 3: Reversible Formation of an Inert Oxide Phase with Active Minority Sites. In order to reproduce the CO flux dependence, we modify model 2 as follows (see Figure 9): We assume that the direct reaction of CO with the oxide takes place at specific sites of high activity only. This active oxide species is consumed by the reaction with adsorbed CO and replenished from the oxide phase. We may speculate that these active sites could, for example, be specific interface sites at the Pd oxide/metal boundary. Similar scenarios have been discussed for the reduction of Rh surface oxides.[3,42] At present, we have to leave the exact nature of these sites open, however, and focus on the kinetics only.

With the above assumptions, we obtain for the CO coverage

$$\frac{d\theta_{CO}}{dt} = \frac{F_{CO}}{N_{Pd}} \cdot S_{CO} - k_{des,CO}\theta_{CO} - k_{LH}\theta_{O(ad)}\theta_{CO} - k_{r,Ox}\theta_{CO}\theta_{O(PdOx,reactive)} \quad (10)$$

The last term in this expression represents the direct reaction of adsorbed CO with the reactive oxide species, which yields for the total CO_2 formation rate

$$r_{CO2} = k_{LH}\theta_{O(ad)}\theta_{CO} + k_{r,Ox}\theta_{CO}\theta_{O(PdOx,reactive)} \quad (11)$$

The changes in the coverage of chemisorbed oxygen on the Pd metal ($\theta_{O(ad)}$), the regular Pd oxide ($\theta_{O(PdOx)}$), and the reactive Pd oxide species ($\theta_{O(PdOx,\ reactive)}$) are described as

$$\frac{d\theta_{O(ad)}}{dt} = 2\frac{F_{O_2}}{N_{Pd}} \cdot S_{O_2} - f_{f,\ Ox}\theta_{O(ad)} + f_{d,Ox}\theta_{*} - k_{LH}\theta_{O(ad)}\theta_{CO} \quad (12)$$

$$\frac{d\theta_{O(PdOx)}}{dt} = f_{f,Ox}\theta_{O(ad)} - f_{d,Ox}\theta_{*} - k_{f,Ox2}\theta_{O(PdOx)} + k_{d,Ox2}\theta_{O(PdOx,reactive)} \quad (13)$$

$$\frac{d\theta_{O\ (PdOx,reactive)}}{dt} = -k_{r,Ox}\theta_{CO}\theta_{O(PdOx,reactive)} + k_{f,Ox2}\theta_{O(PdOx)} - k_{d,Ox2}\theta_{O(PdOx,reactive)} \quad (14)$$

Here, eqs 5 and 6 were used to describe the formation and decomposition rate of the regular Pd oxide. The last two terms in eqs 13 and 14 describe the formation and decomposition of the reactive oxide species.

Model 3 introduces three new parameters, i.e., the rate constants for formation of the reactive oxide species ($k_{f,Ox2}$), for decomposition of the reactive oxide species ($k_{d,Ox2}$), and for CO oxidation involving the reactive oxide phase ($k_{r,Ox}$). Unfortunately, these parameters cannot be independently determined from the experimental data. However, we can take advantage of the fact that the reactive oxide species is a minority species, i.e., its coverage is always low. This fact allows us to apply the pseudo-steady-state assumption for the reactive oxide species

$$\frac{d\theta_{O(PdOx,reactive)}}{dt} \approx 0 \quad (15)$$

yielding, with eq 14 for its concentration,

$$\theta_{O(PdOx,reactive)} \approx \frac{k_{f,Ox2}}{k_{d,Ox2} - k_{r,Ox}\theta_{CO}}\theta_{O(PdOx)} \quad (16)$$

With eq 11 and $k_{eff} = k_{d,Ox2}k_{r,Ox}^{-1}$ we obtain for the reaction rate

$$r_{CO_2} \approx k_{LH}\theta_{O(ad)}\theta_{CO} + \frac{k_{f,Ox2}\theta_{CO}}{k_{eff} - \theta_{CO}} \cdot \theta_{O(PdOx)} \quad (17)$$

The two remaining parameters, $k_{f,Ox2}$ and k_{eff}, can be determined by fitting the model to the PSMB experiments in Figures 6 and 8. We obtain $k_{f,Ox2} = 0.022\ s^{-1}$ and $k_{eff} = 0.05$. A comparison of the experimental results and the simulation using model 3 is shown in Figures 10 and 11. We now find that both types of experiments are reproduced well by the model.

Finally, it should be pointed out that due to the simplicity and the assumptions included in the model, all quantitative results should be treated with care. Still we can conclude that, in addition to the CO oxidation on the metallic part of the Pd particles, the kinetics of the reaction points to a second reaction pathway involving a direct reaction with the oxide. This reaction channel shows a flux dependence, which points to a rather complex reduction mechanism. As the most likely interpretation of this behavior, we introduce a minority species of active sites on the oxide phase. The corresponding microkinetic model is fully compatible with the experimental data.

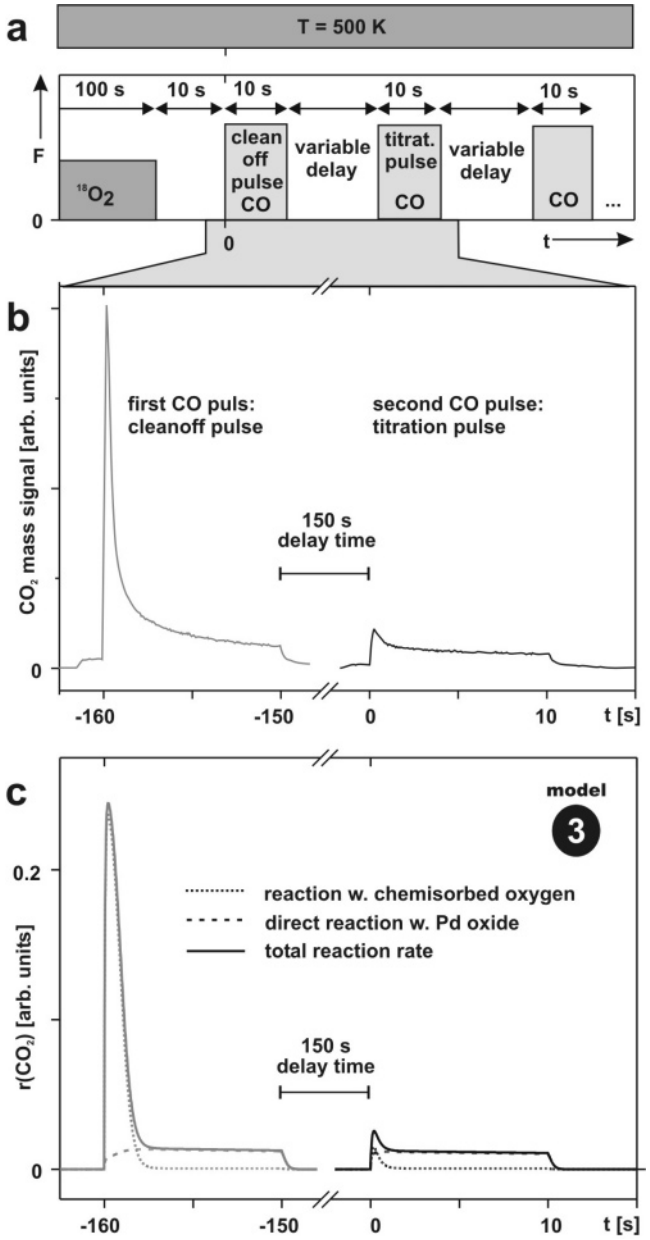

Figure 12. Comparison of the CO_2 production during the first two CO pulses of the PSMB experiment in Figure 8 to the predictions based on microkinetic model 3 (see the text). The dotted and dashed lines represent the reaction channels involving chemisorbed oxygen on metallic Pd and direct reaction with the oxide, respectively.

Finally, it should be stated that the reaction probability for CO impinging on the Pd oxide is much lower than the reaction probability for CO impinging on oxygen-precovered metallic Pd. This difference is illustrated in Figure 12, which shows a direct comparison of the CO_2 production during the first two CO pulses of the PSMB experiment displayed in Figure 8. In Figure 12c, a simulation using model 3 is shown, decomposing

the CO_2 production into the two reaction channels: LH reaction on the Pd metal and direct reaction with the oxide. It is immediately apparent that the reaction on the initially oxygen-precovered sample exceeds the oxide channel by 1−2 orders of magnitude for the pressure range studied here. Only after depletion of chemisorbed oxygen does the direct reaction channel becomes dominant. It follows that, under steady-state conditions, i.e., in a continuous flux of CO and O_2, the LH reaction on the metallic part of the surface can be expected to dominate the total activity, and Pd oxidation primarily leads to a partial deactivation of the catalyst surface. Corresponding effects in steady-state experiments have been discussed in detail in a recent publication.[6] Under transient conditions or under conditions of low oxygen flux, the direct oxide reaction channel may, however, play an important role in the kinetics.

4. Conclusions

We have studied the oxidation and reduction kinetics of Pd nanoparticles on an ordered Fe_3O_4 film as well as the CO oxidation kinetics on partially oxidized Pd nanoparticles. Toward this aim, we employ fully remote-controlled pulse sequence molecular beam (PSMB) experiments, using CO and O_2 beams of variable intensity. These experiments provide detailed information on the mechanism and microkinetics of Pd oxidation/reduction and CO oxidation:

At 500 K and above, large quantities of oxygen (exceeding the O chemisorption capacity by a factor of 4−5) are incorporated into the Pd particles in the form of a Pd oxide phase. Initially, the Pd oxide is formed at the Pd/Fe_3O_4 interface; at higher temperature an increasing fraction of the surface of the Pd particles becomes oxidized as well. Over a broad range of conditions, metallic Pd and Pd oxide phases coexist.

Two reaction regimes are identified by systematic PSMB experiments as a function of oxidation and reaction temperature. In the first regime, corresponding to high coverage of chemisorbed oxygen on metallic Pd, CO oxidation is fast, i.e., the reaction occurs with high reaction probability for CO. In the second regime, i.e., at low oxygen coverage, the kinetics is controlled by reduction of the Pd oxide phase and the reaction probability for CO is low.

The reaction orders with respect to CO are measured by means of PSMB experiments (at CO fluxes from 8.9×10^{12} to 2.6×10^{15} molecules·cm^{-2} s^{-1}). It is found that the Langmuir−Hinshelwood reaction with chemisorbed CO shows the expected first-order dependence in CO, whereas the reduction of the Pd oxide exhibits a complex kinetic behavior with a CO reaction order depending on the CO flux (approximately 0.4−0.6).

PSMB experiments at 500 K show that there is a slow equilibrium between chemisorbed oxygen on the Pd metal and oxygen incorporated into the Pd oxide phases. The rate constants for oxidation and decomposition of the oxide as well as the equilibrium constant are quantitatively determined. At low to intermediate oxidation levels, the equilibrium between both oxygen states strongly favors the Pd oxide. As a consequence, there is a depletion of chemisorbed oxygen from the Pd metal at 500 K and above.

The CO oxidation kinetics on the partially oxidized Pd particles is analyzed in terms of PSMB experiments in combination with microkinetic modeling. It is concluded that the reduction of the Pd oxide is likely to proceed via two competing reaction channels: The first channel occurs via decomposition of the oxide, release of oxygen onto the metal, and reaction of oxygen on Pd metal with CO. The second channel is likely to involve a direct reaction with the oxide, possibly via a minority of active sites of the Pd oxide phase.

Acknowledgment. This work has been funded by the Deutsche Forschungsgemeinschaft (SPP 1091) and the Fonds der Chemischen Industrie. The authors are grateful to D. E. Starr and Sh. K. Shaikhutdinov for providing the STM images.

References and Notes

(1) *Handbook of Heterogeneous Catalysis*; Ertl, G., Knoezinger, H., Weitkamp, J., Eds.; VCH: Weinheim, 1997.

(2) Thomas, J. M.; Thomas, W. J. *Principle and Practice of Heterogeneous Catalysis*; VCH: Weinheim, 1997.

(3) Klikovits, J.; Schmid, M.; Gustafson, J.; Mikkelsen, J.; Resta, A.; Lundgren, E.; Andersen, J. N.; Varga, P. *J. Phys. Chem. B* **2006**, *110*, 9966.

(4) Hendriksen, B. L. M.; Bobaru, S. C.; Frenken, J. W. M. *Top. Catal.* **2005**, *36*, 43.

(5) Schalow, T.; Brandt, B.; Laurin, M.; Guimond, S.; Kuhlenbeck, H.; Schauermann, S.; Libuda, J.; Freund, H.-J. *Surf. Sci.* **2006**, *600*, 2528.

(6) Schalow, T.; Brandt, B.; Laurin, M.; Schauermann, S.; Libuda, J.; Freund, H.-J. *J. Catal.* **2006**, *242*, 58.

(7) Conrad, H.; Ertl, G.; Küppers, J.; Latta, E. E. *Surf. Sci.* **1977**, *65*, 245.

(8) Imbihl, R.; Demuth, J. E. *Surf. Sci.* **1986**, *173*, 395.

(9) Chang, S.-L.; Thiel, P. A. *J. Chem. Phys.* **1988**, *88*, 2071.

(10) Guo, X.; Hoffman, A.; Yates, J. T., Jr. *J. Chem. Phys.* **1989**, *90*, 5787.

(11) Bondzie, V. A.; Kleban, P.; Dwyer, D. J. *Surf. Sci.* **1996**, *347*, 319.

(12) Voogt, E. H.; Mens, A. J. M.; O. L. J. Gijzeman, J. W. G. *Surf. Sci.* **1997**, *373*, 210.

(13) Leisenberger, F. P.; Koller, G.; Sock, M.; Surnev, S.; Ramsey, M. G.; Netzer, F. P.; Klötzer, B.; Hayek, K. *Surf. Sci.* **2000**, *445*, 380.

(14) Bondzie, V. A.; Kleban, P. H.; Dwyer, D. J. *Surf. Sci.* **2000**, *465*, 266.

(15) Zheng, G.; Altman, E. I. *Surf. Sci.* **2000**, *462*, 151.

(16) Zheng, G.; Altman, E. I. *Surf. Sci.* **2002**, *504*, 253.

(17) Lundgren, E.; Kresse, G.; Klein, C.; Borg, M.; Andersen, J. N.; De Santis, M.; Gauthier, Y.; Konvicka, C.; Schmid, M.; Varga, P. *Phys. Rev. Lett.* **2002**, *88*, 246103.

(18) Todorova, M.; Lundgren, E.; Blum, V.; Mikkelsen, A.; Gray, S.; Gustafson, J.; Borg, M.; Rogal, J.; Reuter, K.; Andersen, J. N.; Scheffler, M. *Surf. Sci.* **2003**, *541*, 101.

(19) Lundgren, E.; Gustafson, J.; Mikkelsen, A.; Andersen, J. N.; Stierle, A.; Dosch, H.; Todorova, M.; Rogal, J.; Reuter, K.; Scheffler, M. *Phys. Rev. Lett.* **2004**, *92*, 046101.

(20) Todorova, M.; Reuter, K.; Scheffler, M. *Phys. Rev. B* **2005**, *71*, 195403.

(21) Stierle, A.; Kasper, N.; Dosch, H.; Lundgren, E.; Gustafson, J.; Mikkelsen, A.; Andersen, J. N. *J. Chem. Phys.* **2005**, *122*, 44706.

(22) Schalow, T.; Laurin, M.; Brandt, B.; Schauermann, S.; Guimond, S.; Kuhlenbeck, H.; Starr, D. E.; Shaikhutdinov, S. k.; Libuda, J.; Freund, H.-J. *Angew. Chem., Int. Ed.* **2005**, *44*, 7601.

(23) Schalow, T.; Brandt, B.; Starr, D. E.; Laurin, M.; Schauermann, S.; Shaikhutdinov, S. K.; Libuda, J.; Freund, H.-J. *Catal. Lett.* **2006**, *107*, 189.

(24) Schalow, T.; Brandt, B.; Starr, D. E.; Laurin, M.; Shaikhutdinov, S. K.; Schauermann, S.; Libuda, J.; Freund, H.-J. *Angew. Chem., Int. Ed.* **2006**, *45*, 3775.

(25) Hendriksen, B. L. M.; Bobaru, S. C.; Frenken, J. W. M. *Surf. Sci.* **2004**, *552*, 229.

(26) Zheng, G.; Altmann, E. I. *J. Phys. Chem. B* **2002**, *2002*, 1048.

(27) D'Evelyn, M. P.; Madix, R. J. *Surf. Sci. Rep.* **1984**, *3*, 413.

(28) Asscher, M.; Somorjai, G. A. In *Atomic and Molecular Beam Methods*; Scoles, G., Ed.; Oxford University Press: New York, 1988; Vol. 2, pp 489.

(29) Kleyn, A. W. *Chem. Soc. Rev.* **2003**, *32*, 87.

(30) Libuda, J.; Freund, H.-J. *Surf. Sci. Rep.* **2005**, *57*, 157.

(31) Libuda, J.; Meusel, I.; Hartmann, J.; Freund, H.-J. *Rev. Sci. Instrum.* **2000**, *71*, 4395.

(32) Libuda, J. *Surf. Sci.* **2005**, *587*, 55.

(33) Weiss, W.; Ranke, W. *Prog. Surf. Sci.* **2002**, *70*, 1.

(34) Lemire, C.; Meyer, R.; Henrich, V.; Shaikhutdinov, S. K.; Freund, H.-J. *Surf. Sci.* **2004**, *572*, 103.

(35) Meyer, R.; Shaikhutdinov, S. K.; Freund, H.-J. *Z. Phys. Chem.* **2004**, *218*, 905.
(36) Libuda, J.; Meusel, I.; Hoffmann, J.; Hartmann, J.; Piccolo, L.; Henry, C. R.; Freund, H.-J. *J. Chem. Phys.* **2001**, *114*, 4669.
(37) Hoffmann, J.; Meusel, I.; Hartmann, J.; Libuda, J.; Freund, H.-J. *J. Catal.* **2001**, *204*, 378.
(38) Orent, T. W.; Bader, S. D. *Surf. Sci.* **1982**, *115*, 323.
(39) Engel, T.; Ertl, G. *J. Chem. Phys.* **1978**, *69*, 1267.
(40) Kasper, N.; Stierle, A.; Nolte, P.; Jin-Phillipp, Y.; Wagner, T.; deOteyza, D. G.; Dosch, H. *Surf. Sci.* **2006**, *600*, 2860.
(41) Hoffmann, J.; Schauermann, S.; Johánek, V.; Hartmann, J.; Libuda, J. *J. Catal.* **2003**, *213*, 176.
(42) Lundgren, E.; Gustafson, J.; Resta, A.; Weissenrieder, J.; Mikkelsen, A.; Andersen, J. N.; Köhler, L.; Kresse, G.; Klikovits, J.; Biedermann, A. *J. Electr. Spectr. Rel. Phenom.* **2005**, *144*, 367.